

# Enhanced Kohn-Luttinger topological superconductivity in bands with nontrivial geometry

Ammar Jahin<sup>1</sup> and Shi-Zeng Lin<sup>1,2</sup>

<sup>1</sup>*Theoretical Division, T-4, Los Alamos National Laboratory, Los Alamos, New Mexico 87545, USA*

<sup>2</sup>*Center for Integrated Nanotechnologies (CINT),*

*Los Alamos National Laboratory, Los Alamos, New Mexico 87545, USA*

(Dated: November 15, 2024)

We study the effect of the electron wavefunction on Kohn-Luttinger superconductivity. The role of the wavefunction is encoded in a complex form factor describing the topology and geometry of the bands. We show that the electron wavefunction significantly impacts the superconducting transition temperature and superconducting order parameter. We illustrate this using the lowest Landau level form factor and find exponential enhancement of  $T_c$  for the resulting topological superconductor. We find that the ideal band geometry, which favors a fractional Chern insulator in the flat band limit, has an optimal  $T_c$ . Finally, we apply this understanding to a model relevant to rhombohedral graphene multilayers and unravel the importance of the band geometry for achieving robust superconductivity.

*Introduction.*— The BCS theory is foundational for the understanding of superconductivity. The central equation in the BCS theory is the gap equation, which dictates the pairing symmetry and  $T_c$ . In the standard BCS theory, the gap equation only depends on the Hamiltonian spectrum. Recently, it has been recognized that the wave functions of the Hamiltonian, which encode the system's geometry and topology, also play a crucial role in the problem of superconductivity. For instance, it has been demonstrated both theoretically and experimentally, that the quantum metric provides an additional contribution to the superfluid stiffness and enhance the BKT transition temperature [1–13]. Furthermore, the quantum metric influences the correlation length and upper critical field, as well as the ability to stabilize pairing density waves [5, 14, 15]. The importance of the quantum metric becomes increasingly important, particularly in flat band systems, where the stiffness due to band dispersion is absent.

Moiré superlattice and heterostructure of 2D materials emerge as an important platform to explore the interplay between strong correlations and topology. Superconductivity has been observed in several classes of 2d materials, including twisted bilayer graphene [16–20] and transition metal dichalcogenide (TMD) [21, 22], and graphene multilayers, with valley degree of freedom [23–39]. It is common for superconductivity to arise from the pairing between time-reversal partners, i.e. electrons at opposite valleys. Recently, superconductivity emerging from a spin and valley-polarized normal state has also been observed in tetralayer graphene [40]. While the mechanism for superconductivity in these systems remains under debate [41–45], one particular appealing proposal is the Kohn-Luttinger (KL) mechanism [46] where the pairing of electrons arises merely from the repulsive Coulomb interaction. Motivated by these exciting developments, we study the role of the electron wavefunction on the superconducting transition temperature in the framework of the KL mechanism.

For theoretical description, it is convenient to project the Hamiltonian into a reduced Hilbert space associated with the bands near the Fermi surface. After such projection, the wavefunction enters the projected Hamiltonian through the form factor  $\Lambda(\mathbf{k}, \mathbf{k} + \mathbf{q}) = \langle u_{\mathbf{k}} | u_{\mathbf{k}+\mathbf{q}} \rangle$  with  $|u_{\mathbf{k}}\rangle$  being the periodic part of the Bloch wavefunction. If all we care about is, for example, the superfluid stiffness, defined as a small twist of the superconducting order parameter phase then it is sufficient to consider a small  $\mathbf{q}$  limit, where the quantum geometric tensor describes the norm of the form factor. However, in the KL mechanism for superconductivity, excitation processes with large momentum transfer  $\mathbf{q}$  are also important for screening the Coulomb interaction. This requires keeping the full form factor  $\Lambda(\mathbf{k}, \mathbf{k} + \mathbf{q})$ , not only a small  $\mathbf{q}$  expansion, in the theory description. In general, the KL mechanism generates extremely low  $T_c$ . One way to enhance  $T_c$  is to tune the system close to a van Hove singularity [47]. The central question is how the form factor affects  $T_c$  in the KL mechanism, especially if the geometry of the wavefunction can enhance it.

In this work, we consider the case of the pairing of electrons in a spin and valley-polarized metal without time-reversal symmetry. We partition the form factor corrections to the pairing vertex into its norm  $|\mathcal{W}|$  (defined later), which is gauge invariant, and a gauge-dependent part  $\exp(iF)$ . The norm  $|\mathcal{W}| \leq 1$  is related to the quantum distance in the Hilbert space and controls the screening of the bare Coulomb interaction, as well as act as an overall reduction factor to pairing vertex. The former effect is beneficial to  $T_c$ , while the latter is not. Interestingly, we show that the phase of the form factor splits the degeneracy in the pairing channels with opposite angular momentum, and tends to enhance  $T_c$ . We introduce a toy model with the lowest Landau level (LLL) form factor to illustrate the enhancement of  $T_c$  by several orders of magnitude. We also identified resonance in  $T_c$  associated with the total Berry flux enclosed in the Fermi surface. As a comparison, we compute  $T_c$  in a valley unpolarized sys-

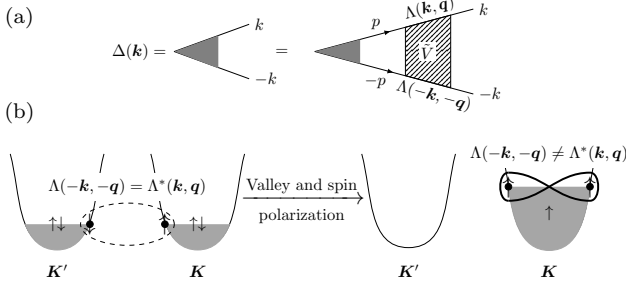


FIG. 1. (a) Linearized gap equation including the effects of band geometry as captured by the form factor  $\Lambda(\mathbf{k}, \mathbf{q})$ . (b) The difference between intervalley pairing and intravalley pairing. The form factor adds a correction to the pairing vertex that is real because of time-reversal symmetry. However in a valley and spin-polarized metals, time-reversal symmetry is broken in the normal state, and the form factors correction is generally complex. This distinction makes both kinds of pairing behave very differently in the presence of nontrivial band geometry.

tem with time-reversal symmetry, where only  $|\mathcal{W}|$  enters into the gap equation. The critical temperature, in this case, is lower, and in some regions, can be lower by orders of magnitude compared to the case without time-reversal symmetry. The screening of the Coulomb interaction depends on dispersion and as well as  $|\mathcal{W}|$ . We show that  $T_c$  is not always enhanced compared to the system with trivial form factor  $|\mathcal{W}| = 1$ , due to the competition between the effect of screening and the reduction of the pairing vertex. Finally, we apply our results to a two-band model describing rhombohedral multilayer graphene.

*Gap equation.*— The band projected Hamiltonian we consider is

$$H = \sum_{\mathbf{k}} (\varepsilon(\mathbf{k}) - \mu) a_{\tau, \mathbf{k}}^\dagger a_{\tau, \mathbf{k}} + \frac{1}{2L^2} \sum_{\mathbf{q}} V(\mathbf{q}) \tilde{\rho}(\mathbf{q}) \tilde{\rho}(-\mathbf{q}), \quad (1)$$

where  $a_{\tau \mathbf{k}}$  annihilate an electron in the band of interest,  $\tau = \pm$  is a valley degree of freedom, and  $\tilde{\rho}(\mathbf{q}) = \sum_{\tau, \mathbf{k}} \Lambda(\mathbf{k}, \mathbf{q}) a_{\tau, \mathbf{k}}^\dagger a_{\tau, \mathbf{k}+\mathbf{q}}$  is the projected density operator and  $L^2$  is the area of the system. We will consider systems with the valley degree of freedom being either fully polarized or unpolarized. We assume the system is either fully spin-polarized on each valley or spin is slaved to the valley as in TMD. We use a gate-screened Coulomb interaction  $V(\mathbf{q}) = 2\pi e^2 \tanh(qd)/\epsilon q$ , where  $d$  is the distance between the gates and the 2D system, and  $\epsilon$  is dielectric permittivity. We use  $d = 36.9$  nm and  $\epsilon = 4\epsilon_0$ , where  $\epsilon_0$  is the vacuum permittivity.

To describe the screening of the bare repulsive interactions between the electrons by the particle-hole fluctuations at the Fermi surface, we use a random phase

approximation (RPA),

$$\tilde{V}(\mathbf{q}) = \frac{V(\mathbf{q})}{1 + \Pi(\mathbf{q})V(\mathbf{q})} \quad (2)$$

where  $\Pi(\mathbf{q})$  is the static polarization operator described by the Lindhard function (defined as a positive number) with the vertices modified by the form factor of the interactions (see supplementary material),

$$\Pi(\mathbf{q}) = -N \int d\mathbf{k} |\Lambda(\mathbf{k}, \mathbf{q})|^2 \frac{f(\varepsilon(\mathbf{k} + \mathbf{q})) - f(\varepsilon(\mathbf{k}))}{\varepsilon(\mathbf{k} + \mathbf{q}) - \varepsilon(\mathbf{k})}, \quad (3)$$

where  $N$  is the number of valleys the electrons occupy, i.e.  $N = 1$  for valley polarized systems and  $N = 2$  for valley unpolarized systems, and  $f(\varepsilon)$  is the Fermi-Dirac distribution function. We look for superconducting instabilities, by studying the linearized gap equation as sketched in Fig. 1 (a), which after summing over the Matsubara frequencies takes the following form,

$$\Delta(\mathbf{k}) = - \log \left( \frac{W}{T_c} \right) \int_{\text{FS}} \frac{dk'_\parallel}{(2\pi)^2 v(\mathbf{k}')} \mathcal{W}(\mathbf{k}, \mathbf{k}') \tilde{V}(\mathbf{k} - \mathbf{k}') \Delta(\mathbf{k}') \quad (4)$$

where  $W$  is the upper energy cut off of the integral, which in our case can be taken to be of the order of the Fermi energy,  $v(\mathbf{k}') = |\partial\varepsilon(\mathbf{k}')/\partial\mathbf{k}'|$ , and we define,

$$\mathcal{W}(\mathbf{k}, \mathbf{k}') = \Lambda(\mathbf{k}, \mathbf{k}' - \mathbf{k}) \Lambda(-\mathbf{k}, -\mathbf{k}' + \mathbf{k}). \quad (5)$$

We note that in the cases with the time-reversal symmetry, and for pairing between electrons on opposite valleys we have  $\Lambda(\mathbf{k}, \mathbf{k}' - \mathbf{k}) = \Lambda^*(-\mathbf{k}, -\mathbf{k}' + \mathbf{k})$ . However, for intravalley pairing, this does not necessarily hold, which we highlight pictorially in Fig. 1 (b). As we will discuss, this can have a big impact on superconductivity.

We focus on systems with a  $U(1)$  rotational symmetry such that both the dispersion and the form factor are invariant under continuous rotations in the plane. In these situations, we can write the gap equation in terms of the angles  $\theta$  and  $\theta'$  between  $\mathbf{k}$  and  $\mathbf{k}'$  and the  $x$ -axis. We find it useful for our discussion to rewrite  $\mathcal{W}(\theta - \theta') = |\mathcal{W}(\theta - \theta')| e^{iF(\theta - \theta')}$ , and define,

$$\mathcal{V}(\theta) = |\mathcal{W}(\theta)| \tilde{V}(\theta) \quad (6)$$

such that the gap equation takes the form

$$\Delta(\theta) = - \log \left( \frac{W}{T_c} \right) \frac{k_f}{v2\pi} \int \frac{d\theta'}{2\pi} e^{iF(\theta - \theta')} \mathcal{V}(\theta - \theta') \Delta(\theta') \quad (7)$$

where we have used  $dk'_\parallel = d\theta' k_f$ . We note that  $|\mathcal{W}(\theta - \theta')|$  is controlled by the quantum distance between states in the Fermi surface, which is captured by the Fubini-study metric for  $|\theta - \theta'| \ll 1$ , whereas the phase  $e^{iF(\theta - \theta')}$  is related to the Berry phase gained as we parallel transport the Bloch wavefunction along the Fermi surface.

Decomposing the gap equation into its angular momentum components, we have

$$\Delta_l = \log\left(\frac{W}{T_c}\right) \lambda_l \Delta_l \quad (8)$$

where we define

$$\Delta_l = \int \frac{d\theta}{2\pi} e^{-i\theta} \Delta(\theta) \quad (9)$$

$$\lambda_l = -\frac{k_f}{v2\pi} \int \frac{d\theta}{2\pi} e^{i(F(\theta)-l\theta)} \mathcal{V}(\theta). \quad (10)$$

In cases with time-reversal symmetry,  $F(\theta) = 0$  and we have  $\lambda_l = \lambda_{-l}$ . Including the complex phase, can break the degeneracy, enhancing one channel while reducing the other, leading to an overall enhancement to  $T_c$ . In fact, in what follows, we describe a situation where the full behavior of the system is governed by the phase factor  $F(\theta)$ . In general, the result of the convolution leading to maximum  $\lambda_l$  is highly nontrivial, since both  $e^{iF(\theta)}$  and the  $\mathcal{V}(\theta)$  will have non-zero components on a wide range of angular momenta.

The form factor appears in two places in the gap equation. It changes the value bubble at non-zero momentum transfer, which changes the renormalization of the interactions. This effect leads to a situation where the energy cost for forward scattering is suppressed compared to the energy cost for scattering with a large momentum transfer, see Fig. 3 (b). This generally means that pairs prefer to “not scatter” rather than scatter off each other, which enhances their chances of forming a pair. However, the effects of band projection also show up as an overall factor  $\mathcal{W}(\theta)$  in the pairing vertex as seen in Eq. (4). Since  $|\mathcal{W}(\theta)| \leq 1$ , this leads to suppression of the critical temperature. This highlights a competition between these two effects, and which one wins depends on the details of the system.

*Lowest Landau level form factor*—The most striking example of the effects of the band geometry is where we have parabolic dispersion  $\varepsilon(\mathbf{k}) = \mathbf{k}^2/(2m)$  in 2D, where the conventional KL mechanism cannot lead to a superconducting instability [48]. The reason is that the polarization bubble is constant  $\Pi(\mathbf{q}) = Nm/(2\pi)$  for all momentum transfers  $q \leq 2k_f$ , and the singularity in 2 (a). It has been shown that this behavior can change if we include trigonal warping effects in the dispersion [49], or corrections to the bubble up to third order in perturbation theory [50]. Here we show that the lowest Landau level (LLL) form factor induces large  $T_c$  in the system. The form factor of the LLL is

$$\Lambda_{\text{LLL}}(\mathbf{k}, \mathbf{q}) = \exp\left[-\frac{B}{4}(q^2 + 2\beta i\mathbf{q} \times \mathbf{k})\right], \quad \beta \leq 1. \quad (11)$$

The LLL form factor has the property that  $|\Lambda_{\text{LLL}}(\mathbf{k}, \mathbf{q})|$  does not depend on  $\mathbf{k}$ , which allows for analytical

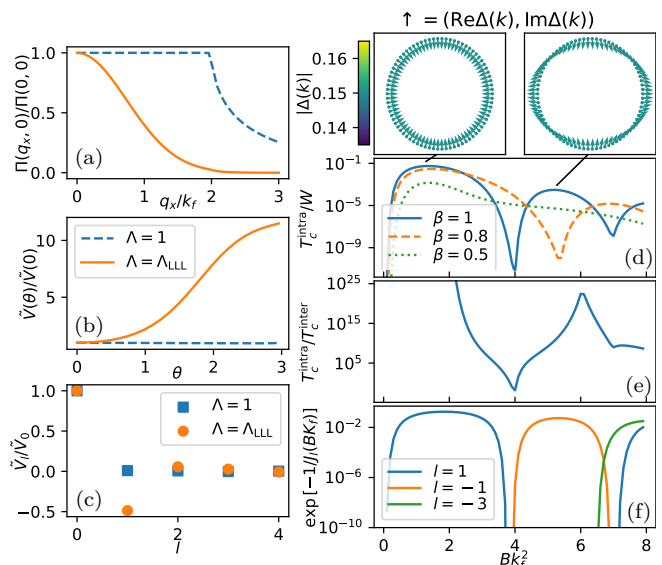


FIG. 2. Effect of band geometry on the bubble (a) and renormalized interactions (b). Panel (c) shows the Fourier transform of the renormalized interactions for different angular momentum channels for the cases with trivial band geometry  $|\mathcal{W}| = 1$  (squares), and non-trivial band geometry (circles). Non-trivial band geometry gives rise to an attractive channel that is otherwise absent. In (d) we plot  $T_c$  for the case of intravalley pairing in units of  $W$  the energy cutoff for various values of  $\beta$ .  $\beta = 1$  corresponds to the ideal band geometry limit, which provides the highest  $T_c$ . Panel (e) compares the critical temperatures of intervalley pairing with intravalley pairing. In this model, intravalley pairing is significantly favored. We can analytically show in the case of large electron mass that the coupling constant for any odd pairing channel is given by the Bessel function, and panel (f) shows that it agrees well with the numerical results of panel (d).

progress. We can immediately show from Eq. (3) that the bubble is not a constant to  $2k_f$ , but rather  $\Pi(\mathbf{q}) \propto e^{-Bq^2/2}$  as shown in Fig. 2 (a). This has a huge effect on the renormalized interactions between electrons at the Fermi surface. In Fig. 2 (b) we plot the renormalized interaction with and without the form factor in solid and dashed lines respectively. Due to the form factor, scattering with high momentum transfers costs more energy than forward scattering, creating attractive channels as shown in Fig. 2 (c). Since we are using a parabolic dispersion, the band geometry guarantees to be favorable for superconductivity.

In Fig. 2 (d) we show  $T_c$  in units of the energy cutoff  $W$  in the case of intravalley pairing. We see clear resonances to  $T_c$  as we increase  $B$ . In the insets, we plot the order parameter around the Fermi surface, for the first two peaks of the ideal limit  $\beta = 1$  plot, showing that the leading instabilities are for angular momentum channels  $l = 1$  and  $l = -1$  respectively at these points. We also show  $T_c$  as we vary  $\beta$  and deviate from the ideal geometry condition. Having ideal geometry is also ideal for super-

conductivity, yielding the highest  $T_c$ . Next, we ask how the effect of band projection differs between intravalley and intervalley pairing. There are two differences between these cases: first,  $\mathcal{W}(\theta)$  in Eq. (7) is complex for intravalley pairing, and real for intervalley pairing, and second, in Eq. (3),  $N = 1$  for intravalley, and  $N = 2$  for intervalley pairing, as we pointed out before. While both intervalley and intravalley pairings have the same qualitative change in the bubble behavior, the intravalley pairing gets a much greater enhancement to  $T_c$  as shown in Fig. 2 (e). The reason for this is that the complex phase  $F(\theta)$  allows for a great enhancement to  $T_c$  in this case.

These results with LLL from factor and parabolic dispersion can be analytically understood in the limit where the mass  $m$  is large such that  $e^{-Bq^2/2}V(\mathbf{q})m/(2\pi) \gg 1$ . Then we can approximate  $\mathcal{V}(\mathbf{q}) = 2\pi/m$ . The coupling constant for every channel is simply given by

$$\lambda_l = - \int \frac{d\theta}{2\pi} e^{-i(Bk_f^2 \sin(\theta) + l\theta)}. \quad (12)$$

The above expression has an analytical form in terms of Bessel functions, which for odd channels relevant for intravalley pairing takes the form,

$$\lambda_l = J_l(\beta Bk_f^2), \quad l \text{ is odd}. \quad (13)$$

The highest  $T_c$  is given by  $Bk_f^2$  corresponding to the maximal of Bessel functions, which is not the simple quantization condition for the total Berry flux enclosed in the Fermi surface,  $B\pi k_f^2 = 2\pi n$ , as one would naively expect. We can also make analytical progress in two other limiting cases, see the supplementary material for more detail.

We caution that the enhancement of  $T_c$  by the band geometry is not universal, which can be illustrated for a quartic band dispersion  $\epsilon(\mathbf{k}) = \gamma\mathbf{k}^4$ , where  $\gamma$  is an energy scale. In Fig. 3 (a) we show the critical temperature of intravalley pairing, as a ratio of the energy cutoff  $T_c^{\text{intra}}/W$  (top) and as a ratio of the critical temperature of intervalley pairing with a trivial form factor  $B = 0$ ,  $T_c^{\text{intra}}/T_{c0}^{\text{inter}}$  (bottom). We see a significant enhancement in  $T_c^{\text{intra}}$  compared to  $T_{c0}^{\text{inter}}$ . This enhancement is mainly attributed to the phase factor  $e^{iF}$ .

For intervalley pairing, we have  $F = 0$ , and similar to the quadratic dispersion case, this reduces the critical temperature compared to the intravalley pairing. In Fig. 3 (b) (top) we plot the intervalley pairing critical temperature as a ratio of the energy cutoff  $T_c^{\text{inter}}/W$ , which shows clearly that the  $T_c^{\text{inter}} \ll T_c^{\text{intra}}$ . Interestingly, comparing  $T_c^{\text{inter}}$  to intervalley pairing with a trivial form factor, we do not get an enhancement of  $T_c$  for all values of  $B$  as shown in Fig. 3 (b) (bottom). This is due the  $\mathcal{W}$  factor in the gap equation (4). Since  $|\mathcal{W}| \leq 1$  it acts to reduce  $T_c$  compared to the cases with no band geometry, and thus  $\mathcal{W} = 1$  identically. We emphasize

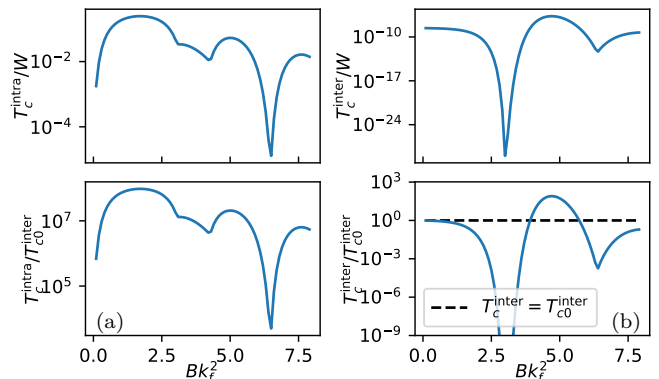


FIG. 3. Superconducting critical temperature using quartic dispersion. The top panels of (a) and (b) show the critical temperature of intravalley pairing  $T_c^{\text{intra}}/W$  and intervalley  $T_c^{\text{inter}}/W$  respectively as a function of  $B$ . Intravalley pairing has a higher critical temperature for all values of  $B$ . The bottom panels show the same quantities but as a ratio of  $T_{c0}^{\text{inter}}$  which is the critical temperature of intervalley pairing with trivial band geometry  $|\mathcal{W}| = 1$ . The case of intravalley pairing with the effects of band geometry always leads to an enhanced  $T_c$ . However, for the intervalley pairing, the effect of band geometry can suppress  $T_c$ .

that in other cases where we do find enhancement, it is because of the effect of band geometry in the bubble showing up in Eq. (3), which tends to increase  $T_c$ . This situation shows that the result of this competition is not universal, and in some scenarios, including the band geometry, it can be bad for superconductivity.

*Two-band model*—A two-band model for the low-energy physics of rhombohedral  $n$ -layer graphene systems can be written as [51]

$$H(\mathbf{k}) = \begin{bmatrix} D & \gamma(k_x + ik_y)^n \\ \gamma(k_x - ik_y)^n & -D \end{bmatrix} - \mu, \quad (14)$$

where  $D$  is a perpendicular displacement field, and  $\gamma$  is an energy scale. The basis of this Hamiltonian is the  $A$  sublattice of the top layer and the  $B$  sublattice of the bottom layer. This Hamiltonian describes a system of electrons with a dispersion  $\epsilon(\mathbf{k}) = \sqrt{\gamma^2 k^{2n} + D^2}$  and the form factor between  $\mathbf{k}$  and  $\mathbf{k}'$  on the Fermi surface as,

$$\Lambda(\mathbf{k}, \mathbf{k}' - \mathbf{k}) = \cos^2(\theta/2) + \sin^2(\theta/2)e^{in\phi}. \quad (15)$$

where,  $\phi$  is the relative angle between  $\mathbf{k}$  and  $\mathbf{k}'$  and  $\cos(\theta) = D/\mu$ .

In Fig. 4 we show the critical temperature for intravalley and intervalley pairing for  $n = 4, 3, 2$ . In all three cases, we fix the size of the Fermi surface determined by electron filling. In the top panels of (a) and (b) we plot  $T_c^{\text{intra}}/W$ , and  $T_c^{\text{inter}}/W$  respectively which show an enhancement to the critical temperature as we increase the number of layers. This effect is mainly due to the density of states (DOS) increase at the Fermi surface as the dispersion gets flatter. Furthermore, there is a general trend for  $T_c$  to increase with increasing displacement

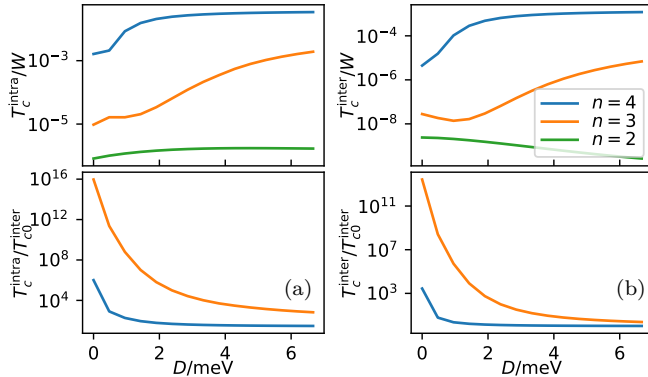


FIG. 4. Results of the effects of band geometry in the two-band model given in Eq. (14) describing rhombohedral  $n$ -layer graphene. The top panels of (a) and (b) show the critical temperature of intravalley pairing  $T_c^{\text{intra}}/W$  and intervalley pairing  $T_c^{\text{inter}}/W$  respectively for  $n = 4, 3, 2$  as a function of the displacement field  $D$ . The Fermi surface size is kept constant in all the plots. As the number of layers gets bigger, the critical temperature is enhanced because the DOS gets bigger as the bands become flatter. Furthermore, there is a general trend for  $T_c$  to increase as we increase the displacement field. This is also a result of the bands getting flatter, increasing the DOS, as the gap increases with  $D$ . The bottom panels show the same quantities but as a ratio of the critical temperature for intervalley pairing with the pseudospin fully polarized, i.e. the form factor is unity across the band. At small displacement fields we see a big enhancement to  $T_c$  that quickly dies out, as the displacement field polarizes the pseudospin.

field, which is again explained by the increase in the DOS at the Fermi surface, since the more gapped the system is the flatter the dispersion. In the lower panels (a) and (b) we plot  $T_c^{\text{intra}}/T_{c0}^{\text{inter}}$ , and  $T_c^{\text{inter}}/T_{c0}^{\text{inter}}$  respectively. Here  $T_{c0}^{\text{inter}}$  is the critical temperature in the case where the pseudospin is fully polarized on either the top or the bottom layer, i.e.  $|\mathcal{W}| = 1$ . The plot shows a large enhancement in the critical temperature due to the band geometry. However, this effect quickly diminishes as the displacement field is increased, polarizing the electrons to the bottom layer. Our calculation shows that the effects of band geometry are washed out at much smaller displacement fields than the values where superconductivity is observed experimentally [40].

*Discussions*—We show that the electron wave function has a significant effect on the critical temperature and pairing symmetry for the KL superconductivity. For a toy model with LLL form factor, there is an exponential enhancement of  $T_c$  depending on the flux enclosed by the Fermi surface. Interestingly,  $T_c$  develops resonance-like features, depending on the total Berry flux enclosed by the Fermi surface. Instead of being quantized to integral of unit quantum flux, we analytically show the condition for the optimal  $T_c$ , which is associated with the maxima of the Bessel functions. The resulting pairing symmetry is chiral  $p \pm ip$  superconductivity, which

hosts Majorana fermion at the vortex core [52–55]. The LLL wave function has unique properties in that it has uniform Berry curvature, and satisfies the trace condition, where the trace of the quantum metric equals the Berry curvature at any momentum [56–58]. The LLL wave function is ideal for realizing the fractional Chern insulators [56, 59–61], and lots of discussions have been devoted to realizing bands with ideal quantum geometry, similar to the LLL [62–64]. In our work, we reveal that the LLL is ideal for achieving topological superconductivity with high  $T_c$  (compared to the Fermi energy).  $T_c$  is highest when the trace condition is satisfied.

We split the form factor into the norm and the phase factor. The norm affects the screening of the repulsive interaction, and generally suppresses the contribution with a small momentum transfer. This is in favor of superconductivity. On the other hand, it also suppresses the magnitude of the pairing vertex which is bad for superconductivity. This results in a competition, which has a non-universal effect on  $T_c$ . Another aspect of the problem is that when time-reversal symmetry is broken, the phase factor splits the otherwise degenerate pairing channels with opposite angular momentum. As a consequence, chiral superconductivity with nontrivial topology is stabilized. To illustrate the role of the form factor without time-reversal symmetry, we compare  $T_c$  with intravalley and intervalley pairing. We find that  $T_c$  for the intravalley pairing is enhanced compared to the intervalley pairing.

Our work therefore points to a promising route to achieve high- $T_c$  topological superconductivity through tuning the band geometry. Our results suggest that a platform for fractional Chern insulators could also be promising for high  $T_c$  topological superconductivity. This seems to align with the experimental fact that both FCI and superconductivity have been observed in graphene multilayers.

The work is partially supported by the U.S. Department of Energy (DOE) National Nuclear Security Administration (NNSA) under Contract No. 89233218CNA000001 through the Laboratory Directed Research and Development (LDRD) Program and was performed, in part, at the Center for Integrated Nanotechnologies, an Office of Science User Facility operated for the DOE Office of Science, under user Proposals No. 2018BU0010 and No. 2018BU0083.

*Note added*—During the preparation of the manuscript, we became aware of a related work, Ref. [65].

[1] S. Peotta and P. Törmä, Superfluidity in topologically nontrivial flat bands, *Nature Communications* **6**, 10.1038/ncomms9944 (2015).

- [2] A. Julku, S. Peotta, T. I. Vanhala, D.-H. Kim, and P. Törmä, Geometric origin of superfluidity in the Lieb-lattice flat band, *Physical Review Letters* **117**, [10.1103/physrevlett.117.045303](#) (2016).
- [3] L. Liang, T. I. Vanhala, S. Peotta, T. Siro, A. Harju, and P. Törmä, Band geometry, Berry curvature, and superfluid weight, *Physical Review B* **95**, [10.1103/physrevb.95.024515](#) (2017).
- [4] X. Hu, T. Hyart, D. I. Pikulin, and E. Rossi, Geometric and conventional contribution to the superfluid weight in twisted bilayer graphene, *Physical Review Letters* **123**, [10.1103/physrevlett.123.237002](#) (2019).
- [5] S. A. Chen and K. Law, Ginzburg-landau theory of flat-band superconductors with quantum metric, *Physical Review Letters* **132**, [10.1103/physrevlett.132.026002](#) (2024).
- [6] H. Tian, X. Gao, Y. Zhang, S. Che, T. Xu, P. Cheung, K. Watanabe, T. Taniguchi, M. Randeria, F. Zhang, C. N. Lau, and M. W. Bockrath, Evidence for Dirac flat band superconductivity enabled by quantum geometry, *Nature* **614**, 440–444 (2023).
- [7] A. Julku, T. J. Peltonen, L. Liang, T. T. Heikkilä, and P. Törmä, Superfluid weight and Berezinskii-Kosterlitz-Thouless transition temperature of twisted bilayer graphene, *Phys. Rev. B* **101**, 060505 (2020).
- [8] F. Xie, Z. Song, B. Lian, and B. A. Bernevig, Topology-bounded superfluid weight in twisted bilayer graphene, *Physical Review Letters* **124**, [10.1103/physrevlett.124.167002](#) (2020).
- [9] P. He, H.-T. Ding, and S.-L. Zhu, Geometry and superfluidity of the flat band in a non-hermitian optical lattice, *Phys. Rev. A* **103**, 043329 (2021).
- [10] J. Herzog-Arbeitman, V. Peri, F. Schindler, S. D. Huber, and B. A. Bernevig, Superfluid weight bounds from symmetry and quantum geometry in flat bands, *Phys. Rev. Lett.* **128**, 087002 (2022).
- [11] P. Törmä, S. Peotta, and B. A. Bernevig, Superconductivity, superfluidity and quantum geometry in twisted multilayer systems, *Nature Reviews Physics* **4**, 528–542 (2022).
- [12] P. Törmä, L. Liang, and S. Peotta, Quantum metric and effective mass of a two-body bound state in a flat band, *Phys. Rev. B* **98**, 220511 (2018).
- [13] K.-E. Huhtinen, J. Herzog-Arbeitman, A. Chew, B. A. Bernevig, and P. Törmä, Revisiting flat band superconductivity: Dependence on minimal quantum metric and band touchings, *Phys. Rev. B* **106**, 014518 (2022).
- [14] J.-X. Hu, S. A. Chen, and K. T. Law, [Anomalous coherence length in superconductors with quantum metric](#) (2024), [arXiv:2308.05686 \[cond-mat.supr-con\]](#).
- [15] Z.-T. Sun, R.-P. Yu, S. A. Chen, J.-X. Hu, and K. T. Law, [Flat-band Fulde-Ferrell-Larkin-Ovchinnikov state from quantum geometry discrepancy](#) (2024), [arXiv:2408.00548 \[cond-mat.supr-con\]](#).
- [16] Y. Cao, V. Fatemi, S. Fang, K. Watanabe, T. Taniguchi, E. Kaxiras, and P. Jarillo-Herrero, Unconventional superconductivity in magic-angle graphene superlattices, *Nature* **556**, 43–50 (2018).
- [17] M. Yankowitz, S. Chen, H. Polshyn, Y. Zhang, K. Watanabe, T. Taniguchi, D. Graf, A. F. Young, and C. R. Dean, Tuning superconductivity in twisted bilayer graphene, *Science* **363**, 1059–1064 (2019).
- [18] X. Lu, P. Stepanov, W. Yang, M. Xie, M. A. Aamir, I. Das, C. Urgell, K. Watanabe, T. Taniguchi, G. Zhang, A. Bachtold, A. H. MacDonald, and D. K. Efetov, Superconductors, orbital magnets and correlated states in magic-angle bilayer graphene, *Nature* **574**, 653–657 (2019).
- [19] G. Chen, A. L. Sharpe, P. Gallagher, I. T. Rosen, E. J. Fox, L. Jiang, B. Lyu, H. Li, K. Watanabe, T. Taniguchi, J. Jung, Z. Shi, D. Goldhaber-Gordon, Y. Zhang, and F. Wang, Signatures of tunable superconductivity in a trilayer graphene moiré superlattice, *Nature* **572**, 215–219 (2019).
- [20] Y. Zhang, G. Shavit, H. Ma, Y. Han, K. Watanabe, T. Taniguchi, D. Hsieh, C. Lewandowski, F. von Oppen, Y. Oreg, and S. Nadj-Perge, [Twist-programmable superconductivity in spin-orbit coupled bilayer graphene](#) (2024), [arXiv:2408.10335 \[cond-mat.supr-con\]](#).
- [21] Y. Xia, Z. Han, K. Watanabe, T. Taniguchi, J. Shan, and K. F. Mak, Unconventional superconductivity in twisted bilayer wse<sub>2</sub>, [arXiv 10.48550/arXiv.2405.14784](#) (2024), [arXiv:2405.14784 \[cond-mat\]](#).
- [22] Y. Guo, J. Pack, J. Swann, L. Holtzman, M. Cothrine, K. Watanabe, T. Taniguchi, D. Mandrus, K. Barmak, J. Hone, A. J. Millis, A. N. Pasupathy, and C. R. Dean, Superconductivity in twisted bilayer wse<sub>2</sub>, [arXiv:2406.03418 \[cond-mat\]](#).
- [23] H. Zhou, T. Xie, T. Taniguchi, K. Watanabe, and A. F. Young, Superconductivity in rhombohedral trilayer graphene, *Nature* **598**, 434–438 (2021).
- [24] Y.-Z. Chou, F. Wu, J. D. Sau, and S. Das Sarma, Acoustic-phonon-mediated superconductivity in rhombohedral trilayer graphene, *Phys. Rev. Lett.* **127**, 187001 (2021).
- [25] T. Li, M. Geier, J. Ingham, and H. D. Scammell, [Higher-order topological superconductivity from repulsive interactions in kagome and honeycomb systems](#) (2022), [arXiv:2108.10897 \[cond-mat.supr-con\]](#).
- [26] A. Ghazaryan, T. Holder, M. Serbyn, and E. Berg, Unconventional superconductivity in systems with annular Fermi surfaces: Application to rhombohedral trilayer graphene, *Physical Review Letters* **127**, [10.1103/physrevlett.127.247001](#) (2021).
- [27] Y.-Z. You and A. Vishwanath, Kohn-Luttinger superconductivity and intervalley coherence in rhombohedral trilayer graphene, *Phys. Rev. B* **105**, 134524 (2022).
- [28] S. Chatterjee, T. Wang, E. Berg, and M. P. Zaletel, Intervalley coherent order and isospin fluctuation mediated superconductivity in rhombohedral trilayer graphene, *Nature Communications* **13**, [10.1038/s41467-022-33561-w](#) (2022).
- [29] A. Jimeno-Pozo, H. Sainz-Cruz, T. Cea, P. A. Pantaleón, and F. Guinea, Superconductivity from electronic interactions and spin-orbit enhancement in bilayer and trilayer graphene, *Phys. Rev. B* **107**, L161106 (2023).
- [30] Z. Li, X. Kuang, A. Jimeno-Pozo, H. Sainz-Cruz, Z. Zhan, S. Yuan, and F. Guinea, Charge fluctuations, phonons, and superconductivity in multilayer graphene, *Phys. Rev. B* **108**, 045404 (2023).
- [31] W. Qin, C. Huang, T. Wolf, N. Wei, I. Blinov, and A. H. MacDonald, Functional renormalization group study of superconductivity in rhombohedral trilayer graphene, *Phys. Rev. Lett.* **130**, 146001 (2023).
- [32] Z. Dong, L. Levitov, and A. V. Chubukov, Superconductivity near spin and valley orders in graphene multilayers, *Phys. Rev. B* **108**, 134503 (2023).

- [33] Z. Dong, Étienne Lantagne-Hurtubise, and J. Alicea, *Superconductivity from spin-canting fluctuations in rhombohedral graphene* (2024), [arXiv:2406.17036](https://arxiv.org/abs/2406.17036) [cond-mat.supr-con].
- [34] H. Zhou, L. Holleis, Y. Saito, L. Cohen, W. Huynh, C. L. Patterson, F. Yang, T. Taniguchi, K. Watanabe, and A. F. Young, Isospin magnetism and spin-polarized superconductivity in bernal bilayer graphene, *Science* **375**, 774–778 (2022).
- [35] Y. Zhang, R. Polski, A. Thomson, E. Lantagne-Hurtubise, C. Lewandowski, H. Zhou, K. Watanabe, T. Taniguchi, J. Alicea, and S. Nadj-Perge, Enhanced superconductivity in spin-orbit proximitized bilayer graphene, *Nature* **613**, 268–273 (2023).
- [36] C. Li, F. Xu, B. Li, J. Li, G. Li, K. Watanabe, T. Taniguchi, B. Tong, J. Shen, L. Lu, J. Jia, F. Wu, X. Liu, and T. Li, Tunable superconductivity in electron- and hole-doped bernal bilayer graphene, *Nature* **631**, 300–306 (2024).
- [37] T. Cea, P. A. Pantaleón, V. o. T. Phong, and F. Guinea, Superconductivity from repulsive interactions in rhombohedral trilayer graphene: A kohn-luttinger-like mechanism, *Phys. Rev. B* **105**, 075432 (2022).
- [38] Y.-Z. Chou, F. Wu, J. D. Sau, and S. Das Sarma, Acoustic-phonon-mediated superconductivity in bernal bilayer graphene, *Phys. Rev. B* **105**, L100503 (2022).
- [39] Z. Dong, A. V. Chubukov, and L. Levitov, Transformer spin-triplet superconductivity at the onset of isospin order in bilayer graphene, *Phys. Rev. B* **107**, 174512 (2023).
- [40] T. Han, Z. Lu, Y. Yao, L. Shi, J. Yang, J. Seo, S. Ye, Z. Wu, M. Zhou, H. Liu, G. Shi, Z. Hua, K. Watanabe, T. Taniguchi, P. Xiong, L. Fu, and L. Ju, *Signatures of chiral superconductivity in rhombohedral graphene* (2024), [arXiv:2408.15233](https://arxiv.org/abs/2408.15233) [cond-mat.mes-hall].
- [41] Y.-Z. Chou, J. Zhu, and S. D. Sarma, *Intravalley spin-polarized superconductivity in rhombohedral tetralayer graphene* (2024), [arXiv:2409.06701](https://arxiv.org/abs/2409.06701) [cond-mat.supr-con].
- [42] M. Geier, M. Davydova, and L. Fu, *Chiral and topological superconductivity in isospin polarized multilayer graphene* (2024), [arXiv:2409.13829](https://arxiv.org/abs/2409.13829) [cond-mat.supr-con].
- [43] Y.-T. Hsu, A. Vaezi, M. H. Fischer, and E.-A. Kim, Topological superconductivity in monolayer transition metal dichalcogenides, *Nature Communications* **8**, 14985 (2017).
- [44] Y.-Q. Wang, Z.-Q. Gao, and H. Yang, Chiral superconductivity from parent chern band and its non-abelian generalization, [arXiv 10.48550/arXiv.2410.05384](https://arxiv.org/abs/2410.05384) (2024), [arXiv:2410.05384](https://arxiv.org/abs/2410.05384) [cond-mat].
- [45] H. Yang and Y.-H. Zhang, Topological incommensurate fulde-ferrell-larkin-ovchinnikov superconductor and bogoliubov fermi surface in rhombohedral tetralayer graphene, [arXiv 10.48550/arXiv.2411.02503](https://arxiv.org/abs/2411.02503) (2024), [arXiv:2411.02503](https://arxiv.org/abs/2411.02503) [cond-mat].
- [46] W. Kohn and J. M. Luttinger, New mechanism for superconductivity, *Phys. Rev. Lett.* **15**, 524 (1965).
- [47] R. Nandkishore, R. Thomale, and A. V. Chubukov, Superconductivity from weak repulsion in hexagonal lattice systems, *Physical Review B* **89**, 10.1103/physrevb.89.144501 (2014).
- [48] M. Y. Kagan, V. A. Mitskan, and M. M. Korovushkin, Anomalous superconductivity and superfluidity in repulsive fermion systems, *Uspekhi Fizicheskikh Nauk* **185**, 785–815 (2015).
- [49] M. A. Baranov and M. Y. Kagan, D-wave pairing in the two-dimensional hubbard model with low filling, *Zeitschrift für Physik B Condensed Matter* **86**, 237–239 (1992).
- [50] A. V. Chubukov, Kohn-luttinger effect and the instability of a two-dimensional repulsive fermi liquid at  $t=0$ , *Phys. Rev. B* **48**, 1097 (1993).
- [51] S. Slizovskiy, E. McCann, M. Koshino, and V. I. Fal'ko, Films of rhombohedral graphite as two-dimensional topological semimetals, *Communications Physics* **2**, 10.1038/s42005-019-0268-8 (2019).
- [52] J. Alicea, New directions in the pursuit of majorana fermions in solid state systems, *Reports on Progress in Physics* **75**, 076501 (2012).
- [53] C. Kallin and J. Berlinsky, Chiral superconductors, *Reports on Progress in Physics* **79**, 054502 (2016).
- [54] N. Read and D. Green, Paired states of fermions in two dimensions with breaking of parity and time-reversal symmetries and the fractional quantum hall effect, *Phys. Rev. B* **61**, 10267 (2000).
- [55] M. Sato and Y. Ando, Topological superconductors: a review, *Reports on Progress in Physics* **80**, 076501 (2017).
- [56] R. Roy, Band geometry of fractional topological insulators, *Phys. Rev. B* **90**, 165139 (2014).
- [57] S. A. Parameswaran, R. Roy, and S. L. Sondhi, Fractional quantum hall physics in topological flat bands, *Comptes Rendus. Physique* **14**, 816–839 (2013).
- [58] J. Wang, J. Cano, A. J. Millis, Z. Liu, and B. Yang, Exact landau level description of geometry and interaction in a flatband, *Phys. Rev. Lett.* **127**, 246403 (2021).
- [59] Y.-H. Wu, J. K. Jain, and K. Sun, Adiabatic continuity between hofstadter and chern insulator states, *Phys. Rev. B* **86**, 165129 (2012).
- [60] P. J. Ledwith, G. Tarnopolsky, E. Khalaf, and A. Vishwanath, Fractional chern insulator states in twisted bilayer graphene: An analytical approach, *Phys. Rev. Res.* **2**, 023237 (2020).
- [61] B. Mera and T. Ozawa, Engineering geometrically flat chern bands with fubini-study kähler structure, *Phys. Rev. B* **104**, 115160 (2021).
- [62] P. J. Ledwith, A. Vishwanath, and E. Khalaf, Family of ideal chern flatbands with arbitrary chern number in chiral twisted graphene multilayers, *Phys. Rev. Lett.* **128**, 176404 (2022).
- [63] X. Wan, S. Sarkar, S.-Z. Lin, and K. Sun, Topological exact flat bands in two-dimensional materials under periodic strain, *Phys. Rev. Lett.* **130**, 216401 (2023).
- [64] S. A. A. Ghorashi, A. Dunbrack, A. Abouelkomsan, J. Sun, X. Du, and J. Cano, Topological and stacked flat bands in bilayer graphene with a superlattice potential, *Phys. Rev. Lett.* **130**, 196201 (2023).
- [65] G. Shavit and J. Alicea, Quantum geometric unconventional superconductivity, [arXiv 10.48550/arXiv.2411.05071](https://arxiv.org/abs/2411.05071) (2024), [arXiv:2411.05071](https://arxiv.org/abs/2411.05071) [cond-mat].
- [66] J. S. Hofmann, D. Chowdhury, S. A. Kivelson, and E. Berg, Heuristic bounds on superconductivity and how to exceed them, *npj Quantum Materials* **7**, 10.1038/s41535-022-00491-1 (2022).

# Supplementary materials for “Enhanced Kohn-Luttinger topological superconductivity in bands with nontrivial geometry”

Ammar Jahin<sup>1</sup> and Shi-Zeng Lin<sup>1,2</sup>

<sup>1</sup>*Theoretical Division, T-4, Los Alamos National Laboratory, Los Alamos, New Mexico 87545, USA*

<sup>2</sup>*Center for Integrated Nanotechnologies (CINT),*

*Los Alamos National Laboratory, Los Alamos, New Mexico 87545, USA*

(Dated: November 15, 2024)

## Linearized gap equation and the randomized phase approximation

We follow the approach outlined in Ref. [26] for the renormalization of the interactions. We use a random phase approximation which is controlled by a  $1/N$  expansion,  $N$  being the number of fermion species, as we sum over the ladder of bubbles as shown in Fig. 1. This gives us the renormalized interactions  $\mathcal{W}(\mathbf{k}, \mathbf{k}')\tilde{V}(\mathbf{q})$  in the linearized gap equation as written in Eq. (4) in the main text.

To facilitate the numerical evaluation of the eigenvalue problem of the linearized gap equation, we divide the Fermi surface into equal segments and convert the integral equation into a matrix equation,

$$\Delta_{\mathbf{k}} = -\log\left(\frac{W}{T_c}\right) \sum_{\mathbf{k}'} \frac{\delta k'}{(2\pi)^2 v_{\mathbf{k}'}} \mathcal{W}_{\mathbf{k}, \mathbf{k}'} \tilde{V}_{\mathbf{k}, \mathbf{k}'} \Delta_{\mathbf{k}'} \quad (\text{S1})$$

where  $\delta k$  is the size of the individual piece on the Fermi surface used in the calculation. We further define the normalized order parameter  $\bar{\Delta}_{\mathbf{k}} = \sqrt{\frac{\delta k}{v_{\mathbf{k}}}} \Delta_{\mathbf{k}}$ , which gives us the symmetric equation,

$$\bar{\Delta}_{\mathbf{k}} = -\log\left(\frac{W}{T_c}\right) \sum_{\mathbf{k}'} \frac{1}{(2\pi)^2} \sqrt{\frac{\delta k \delta k'}{v_{\mathbf{k}} v_{\mathbf{k}'}}} \mathcal{W}_{\mathbf{k}, \mathbf{k}'} \tilde{V}_{\mathbf{k}, \mathbf{k}'} \Delta_{\mathbf{k}'} = \sum_{\mathbf{k}'} \log\left(\frac{W}{T_c}\right) \mathcal{M}_{\mathbf{k}, \mathbf{k}'} \bar{\Delta}_{\mathbf{k}'} \quad (\text{S2})$$

where the matrix  $\mathcal{M}$  is Hermitian. It is this matrix that we diagonalize and look for its biggest eigenvalue  $\lambda_{\max}$  whose eigenvector has an odd angular momentum for the case of intravalley pairing, or even or odd for the case of intervalley pairing.

Finally, we comment on our bubble calculation. We use a grid in momentum space whose dimensions is five times as large as the Fermi surface in either directions. We divide this interval into a grid of  $6000 \times 6000$ . Ultimately, we need to use a finite temperature, to evaluate the bubble. We use a temperature that is of the order of  $v_{\mathbf{k}} \delta k_{\text{grid}}$ , where  $\delta k_{\text{grid}}$  is the linear size of the grid.

## Analysis of critical temperature for parabolic dispersion

### Lowest Landau level

In the main text, we showed how we can make analytical progress in the case of large mass. Here we give the details of the proof in the main text as well as show two more cases where analytical progress can be made using the LLL form factor.

In the main text, we made use of the following identity,

$$e^{\pm iz \sin(\phi)} = J_0(z) + 2 \sum_{n=1}^{\infty} J_{2n}(z) \cos(2n\theta) \pm 2i \sum_{n=1}^{\infty} J_{2n+1}(z) \sin((2n+1)\theta), \quad (\text{S3})$$

so that we have

$$\int \frac{d\phi}{2\pi} e^{-i\ell\phi} e^{-iBk_f^2 \sin(\phi)} = (-1)^\ell J_\ell(Bk_f^2). \quad (\text{S4})$$

Focusing on the odd pairing channels, we arrive at the coupling constant  $\lambda_l$  given in Eq. (13) of the main text.



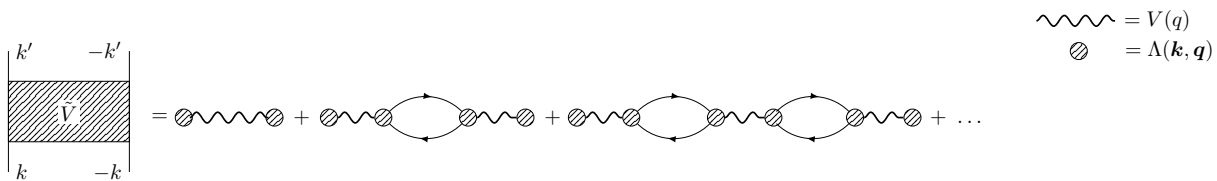


FIG. 1. The renormalized interactions under the random phase approximation. We modify every vertex to include the effects of band projection.

We can also obtain an analytical expression for the critical temperature if we (1) use a parabolic dispersion  $\varepsilon(\mathbf{k}) = \mathbf{k}^2/(2m)$ , (2) assume an on-site bare interaction, so that  $V(q) = U$ , and (3) take  $\beta = 0$  in the LLL form factor. In this case, we can write

$$\mathcal{V}(\phi) = \frac{U e^{-Bk_f^2(1-\cos(\phi))}}{1 + \frac{mU}{2\pi} e^{-Bk_f^2(1-\cos(\phi))}} \quad (\text{S5})$$

To simplify the notation we define,  $\alpha = mU/(2\pi)e^{-Bk_f^2}$ , and expand the denominator,

$$\mathcal{V}(\phi) = \sum_{n=1}^{\infty} (-\alpha)^n e^{nBk_f^2 \cos(\phi)}. \quad (\text{S6})$$

We make use of the identity

$$e^{z \cos(\phi)} = I_0(z) + 2 \sum_{l=1}^{\infty} I_l(z) \cos(l\phi) = \sum_{l=-\infty}^{\infty} I_l(z) e^{il\phi}, \quad (\text{S7})$$

where  $I_l(z)$  are the modified Bessel functions, and we used the fact that  $I_{-l}(z) = I_l(z)$  in the last equality. We thus arrive at the following expression for the coupling constant at each channel,

$$\lambda_l = - \sum_{n=1}^{\infty} (-\alpha)^n I_l(nBk_f^2). \quad (\text{S8})$$

Even in this case of real  $\mathcal{W}$ , we can have attractive channels even using a parabolic dispersion.

Finally, we consider a case where the renormalized interactions decay very rapidly with the momentum transfer  $\mathbf{q}$  so that we can take  $\mathcal{V}(\phi) = \mathcal{V}_0 \delta(\phi)$ . In this case we can write,

$$\lambda_l = - \frac{m}{2\pi} \mathcal{V}_0 \int \frac{d\phi}{2\pi} = - \frac{m}{2\pi}. \quad (\text{S9})$$

Thus we have all channels being repulsive. Perhaps this is not surprising, since such renormalized interaction has an infinite range in real space, and thus impossible to have an attractive channel.

### Two band model for tetralayer graphene

In the main text, we considered a two-band model that describes  $n$ -layers of rhombohedral graphene with a displacement field  $D$  applied perpendicular to the plane of the sample [51]. For this model, we can show that the critical temperature for intervalley and intravalley pairing are equal when  $D = 0$ , and using the same bubble in both cases. For this model we can write down the form factor for  $\mathbf{k}$  and  $\mathbf{k}'$  on the Fermi surface as,

$$\Lambda(\theta, \phi) = \cos^2(\theta/2) + \sin^2(\theta/2) e^{in\phi}, \quad \mathbf{k}, \mathbf{k}' \text{ on Fermi surface.} \quad (\text{S10})$$

where,  $\phi$  is the relative angle between  $\mathbf{k}$  and  $\mathbf{k}'$  in the  $xy$ -plane, and  $\cos(\theta) = D/\mu$ . In general, we have

$$\lambda_l = - \sum_{l'} \mathcal{W}_{l-l'} \tilde{V}_{l'}. \quad (\text{S11})$$

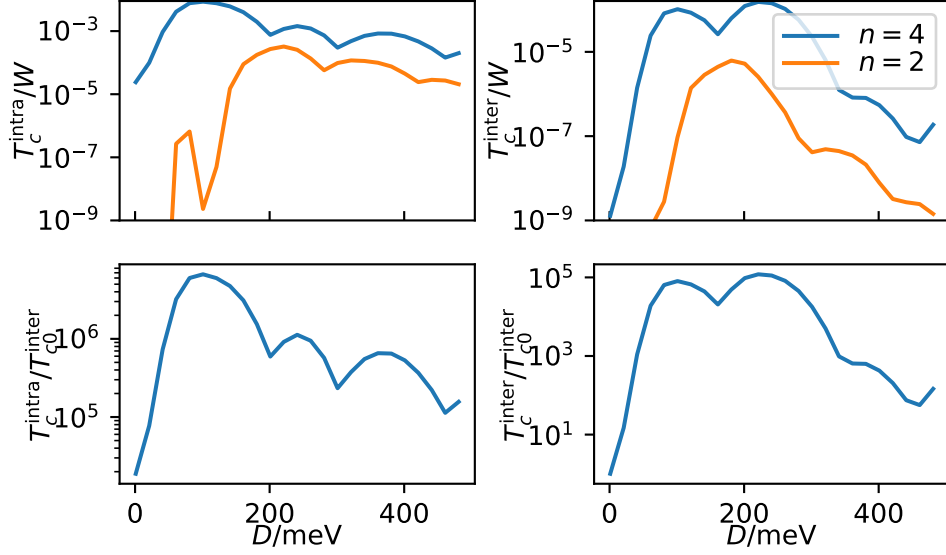


FIG. 2. Results of the effects of band projection for the  $\zeta$ -lattice defined in Ref. [66].  $T_c^{\text{intra}}$  is the critical temperature in a valley polarized setting and thus intravalley pairing, while  $T_c^{\text{inter}}$  is the critical temperature for intervalley pairing.  $T_{c0}^{\text{inter}}$  represents the critical temperature for intervalley coupling with all the vectors are polarized in the same direction on the Fermi surface.

For intravalley pairing, we can write down,

$$\mathcal{W}^{\text{intra}}(\theta, \phi) = [\Lambda(\theta, \phi)]^2 = \cos^4(\theta/2) + 2\sin^2(\theta/2)\cos^2(\theta/2)e^{in\phi} + \sin^4(\theta/2)e^{i2n\phi} \quad (\text{S12})$$

while for intervalley pairing we have

$$\mathcal{W}^{\text{inter}}(\phi) = |\Lambda(\theta, \phi)|^2 = \cos^4(\theta/2) + \sin^4(\theta/2) + \sin^2(\theta/2)\cos^2(\theta/2)(e^{in\phi} + e^{-in\phi}) \quad (\text{S13})$$

For the case when  $D = 0$ , or  $\theta = \pi$  we have,

$$\mathcal{W}^{\text{intra}}(\phi) = \frac{e^{in\phi}}{4} (e^{-in\phi} + 2 + e^{in\phi}) = e^{in\phi} \mathcal{W}^{\text{inter}}(\phi) \quad (\text{S14})$$

and thus,

$$\mathcal{W}_{l+n}^{\text{intra}} = \mathcal{W}_l^{\text{inter}}. \quad (\text{S15})$$

Thus in a situation where  $\tilde{V}_l$  are the same for intervalley and intravalley pairing we have  $\lambda_l^{\text{intra}} = \lambda_{l-n}^{\text{inter}}$ . However, in most situations,  $\tilde{V}_l$  differs between the two cases because the polarization bubble in the case of intervalley pairing is double that of the bubble in the case of intravalley pairing.

### zeta lattice results

Ref. [66] introduced a model with exact flat bands, and a tunable quantum metric, controlled by the parameter  $\zeta$ . The Hamiltonian of such model is given by

$$H(\mathbf{k}) = -t(\sin(\alpha(\mathbf{k}))\sigma_x + \cos(\alpha(\mathbf{k}))\sigma_y) \quad (\text{S16})$$

$$\alpha(\mathbf{k}) = \zeta(\cos(k_x) + \cos(k_y)), \quad (\text{S17})$$

where  $\sigma_x$  and  $\sigma_y$  are the Pauli matrices. This model is interesting in that the Berry curvature vanishes for all points in the Brillouin zone. This makes the model interesting in isolating the effects of the quantum metric on  $T_c$ . We have already seen an enhancement is possible for the LLL from factor when  $\beta = 0$ , corresponding to vanishing Berry

curvature. Is this effect also true for other models with zero Berry curvature? We take this model as an additional data point. We calculate the form factor using the following expression for the periodic part of Bloch wavefunctions

$$|u(\mathbf{k})\rangle = \frac{1}{\sqrt{2}} \begin{bmatrix} 1 \\ e^{i\alpha(\mathbf{k})} \end{bmatrix}. \quad (\text{S18})$$

Furthermore, to facilitate the calculation of  $T_c$  we endow each band with a dispersion,

$$\varepsilon(\mathbf{k}) = \gamma \left( \frac{k}{k_0} \right)^n \quad (\text{S19})$$

where  $\gamma$  and  $k_0$  set the overall scale of energy and momentum respectively.

In Fig 2 we show results for the critical temperature for  $n = 2$ , and 4. In the case of  $n = 2$ , we also see that the effects of band projection allow for superconductivity when it would not be there otherwise. We also see resonance peaks in the critical temperature reminiscent to those seen in the LLL case. For the  $n = 4$  dispersion, we comparing the critical temperatures of intravalley and intervalley with band projection, to the expected critical temperature when we ignore the effects of band projection. We find enhancement to the critical temperature in both cases. This is unlike the LLL case where the effect of band projection is bad for  $T_c$  in the case of intervalley pairing.